(Received 25 May 2025, Accepted 3 September 2025, Scheduled 15 September 2025)

A Compact 4-Ports UWB MIMO Antenna with WiMAX and WLAN Band Rejection Characteristics

Maher M. El Tayeb[1], Deena A. El Hamid Salem[2], Ali R. Mahmoud[3], Imran Mohd Ibrahim[4], Ahmed J. A. Al-Gburi[4,*], and Mohamed H. M. Mahmoud[5]

[1] *Communications and Electronics Department, MSA University, 6 October, Egypt*
[2] *Center of Teaching and Learning, University of Regina, Canada*
[3] *Ahram Canadian University, 6 October, Cairo, Egypt*
[4] *Center for Telecommunication Research & Innovation (CeTRI)*
Fakulti Teknologi Dan Kejuruteraan Elektronik Dan Komputer (FTKEK)
Universiti Teknikal Malaysia Melaka (UTeM)
Jalan Hang Tuah Jaya, Durian Tunggal, Melaka 76100, Malaysia
[5] *Communications and Electronics Department, Giza Engineering Institute, Egypt*

ABSTRACT: This study introduces a compact four-port UWB MIMO antenna featuring dual-band rejection capabilities aimed at suppressing interference from coexisting wireless services, specifically WiMAX at 3.5 GHz and WLAN at 5.5 GHz. The antenna employs an inverted C-slot etched into the radiator to achieve the WiMAX notch, while EBG structures are integrated to enable suppression of the WLAN band at 5.5 GHz. Fabricated on a low-cost FR4 substrate with dimensions $52 \times 52 \times 1.5\,\text{mm}^3$ ($\varepsilon_r = 4.5$), the proposed design achieves high port isolation exceeding 15 dB across the 3.1–10.6 GHz UWB range. Simulated results show an operational bandwidth from 3 to 11 GHz, extending beyond 12 GHz in measurements, without the need for additional filters or decoupling structures. The antenna exhibits quasi-omnidirectional radiation patterns with a peak gain of 7.2 dBi and significant gain suppression at the notch frequencies (-1.5 dBi at 3.5 GHz and -1.2 dBi at 5.5 GHz). It maintains a VSWR below 2 across the UWB and achieves radiation efficiency above 90% outside the notched bands. The envelope correlation coefficient remains below 0.005, enabling a high diversity gain approaching 10 dB. The EBG structures effectively reduce mutual coupling, allowing a compact element spacing of just 2 mm (approximately $\lambda/12.5$ at 12 GHz). Both simulation and measurement results validate the proposed design's suitability for mitigating co-channel interference in UWB-MIMO applications, including satellite communications in the S/C/X bands and high-speed wireless systems.

1. INTRODUCTION

Ultra-wideband (UWB) communication systems operating in the 3.1–10.6 GHz band under the Federal Communications Commission [1] have become vital for high-speed wireless applications — from short-range links and IoT to body area and personal area networks [2, 3]. Their appeal lies in large fractional bandwidth, low spectral power density, and immunity to multipath fading [4, 5]. Yet, inherent issues like severe multipath and narrowband interference have driven the adoption of multi-input multi-output (MIMO) configurations to boost capacity and reliability [6, 7]. Despite these benefits, designing compact UWB MIMO antennas presents technical challenges. Requirements include small size, high isolation ($>$ 20 dB), and in-band interference suppression from coexisting services like WiMAX (3.5 GHz) and WLAN (5.5 GHz) [8, 9]. Meeting them simultaneously introduces trade-offs: closely spaced elements raise mutual coupling, while embedded notching can impair impedance matching and radiation uniformity [10, 11]. To address this, recent studies integrate advanced decoupling and band-notch structures directly into antenna geometries, avoiding external filters [12, 13]. This work proposes a compact 4-port UWB MIMO antenna with dual-band notches for WiMAX and WLAN suppression. Using inverted C-slots and electromagnetic band gap (EBG) structures, the design achieves isolation over 18 dB, with suppression confirmed via simulations and measurements. Although values above 20 dB are generally preferred, isolation levels around 18 dB have been reported as acceptable in several recent UWB MIMO designs, especially when being balanced with compact size and notching performance. This aligns with trends toward compact antennas for high-speed wireless systems in wearable, 5G, and satellite platforms [14–18].

1.1. Band Notching Techniques

Suppressing in-band interference like WiMAX and WLAN is essential for UWB MIMO systems. C- or U-shaped slots in radiators or ground planes are widely used for their tunability and design simplicity [4, 23]. A dual-notch design with an inverted C-slot and parasitic strips achieved this without compromising broadband matching [13]. Complementary split-ring resonators (CSRRs) offer compact, high-Q notches. In [5], triple band-stop filters at 2.8–3.85, 5.11–5.98, and 7.34–8.69 GHz were realized using CSRRs on a flexible substrate. Some designs combined CSRRs with stubs or parasitic elements for

* Corresponding author: Ahmed Jamal Abdullah Al-Gburi (ahmedjamal@ieee.org, ahmedjamal@utem.edu.my).

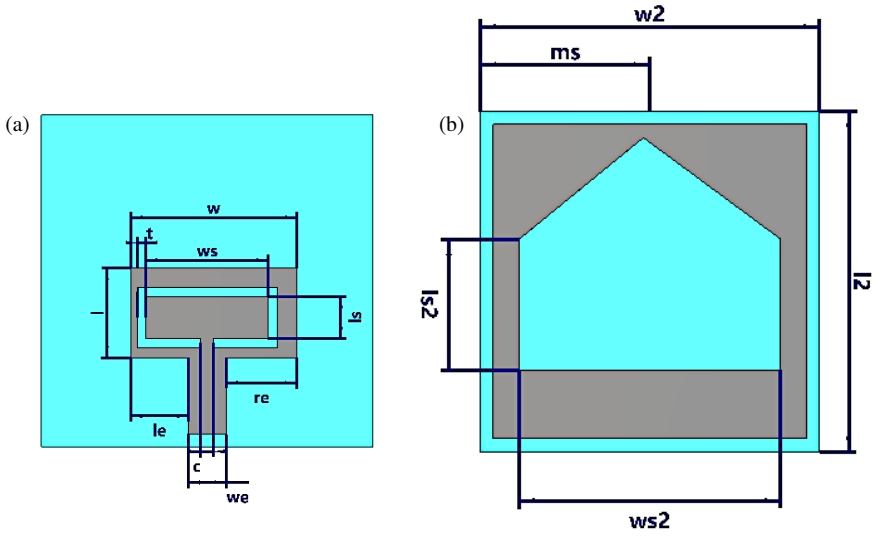

FIGURE 1. Single antenna. (a) Top view. (b) Back view.

greater flexibility [24, 25]. More recent 4-port layouts integrate them directly into the antenna. In [26], etched slots and backplane stubs produced precise notches at WiMAX and WLAN bands, with minimal distortion. Such implementations are validated through S_{11} and voltage standing wave ratio (VSWR) measurements, where VSWR typically exceeds 6 at the notched frequencies [27].

1.2. Recent Advances in UWB MIMO Designs

Reducing mutual coupling in dense MIMO arrays has led to several effective strategies. Defected ground structures (DGSs), such as L-shaped or serpentine slots, interrupt surface currents and achieve $>$ 20 dB isolation [9, 19]. A fan-shaped isolator yielded $>$ 15 dB isolation from 2 to 11 GHz [1], while combining DGS with neutralization lines achieved $>$ 22 dB in quad-port UWB designs [3, 20]. Electromagnetic band gap (EBG) elements and frequency selective surfaces (FSSs) also manipulate current flow. In [2], octagonal EBGs provided both decoupling and frequency notching. Neutralization lines and stub-loaded resonators have been used between ports to redirect surface currents and enhance isolation [14, 21]. Another effective approach is polarization diversity — placing elements orthogonally — which reduced coupling by $>$ 22 dB in [7]. Flexible and textile-based antennas have adapted these principles for wearable use, achieving reliable isolation [15, 22]. A $46 \times 41\,\text{mm}^2$ antenna in [3] achieved dual notches at 5.5 and 8 GHz through hybrid DGS-neutralization decoupling. Triple notches in a $47 \times 47\,\text{mm}^2$ array were achieved in [2] through U-slots and a fan-shaped isolator. Flexible antennas, including [5]'s antenna based on an liquid crystal polymer (LCP) substrate, showcase the incorporation of triple notches and $>$ 22 dB isolation, highlighting wearable IoT potential. Ref. [1] minimized a 4-port array into $36 \times 36\,\text{mm}^2$ while ensuring broadband performance (2–11 GHz). Results show that the proposed antenna provides double notches while an isolation of at least 15 dB is gained.

2. SINGLE UWB ANTENNA UNIT

The single antenna unit, introduced in our earlier work [6], is shown in Fig. 1. It is a compact UWB antenna incorporating a WLAN notch achieved through an inverted C-shaped slot embedded into the radiating patch, forming the core element of the MIMO antenna system proposed in this work. The design parameters for this unit antenna are provided in millimeters, with detailed dimensions summarized in Table 1.

2.1. Performance Evaluation

2.1.1. Reflection Coefficient (S_{11})

The simulated and measured reflection coefficients (S_{11}) of our developed antenna are presented in Fig. 2. The result shows that there is a good agreement between simulation and measurement, which confirms that the antenna achieves S_{11} levels below -10 dB over a very wide band — approximately 2.6 GHz to more than 12 GHz — and demonstrates good impedance matching and ultra-wideband (UWB) behavior.

Two clear notches lie around 3.5 GHz and 5.5 GHz, where S_{11} is well below -30 dB, indicating high resonance and good

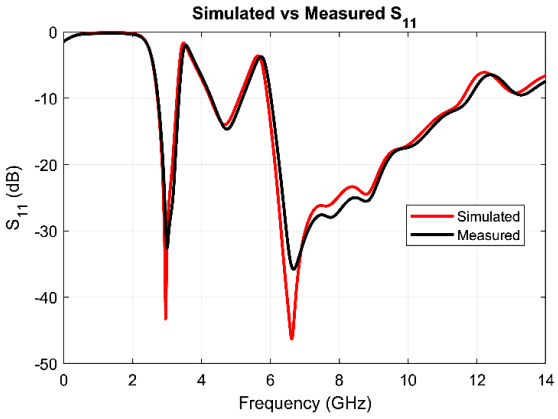

FIGURE 2. Performance of the single UWB antenna.

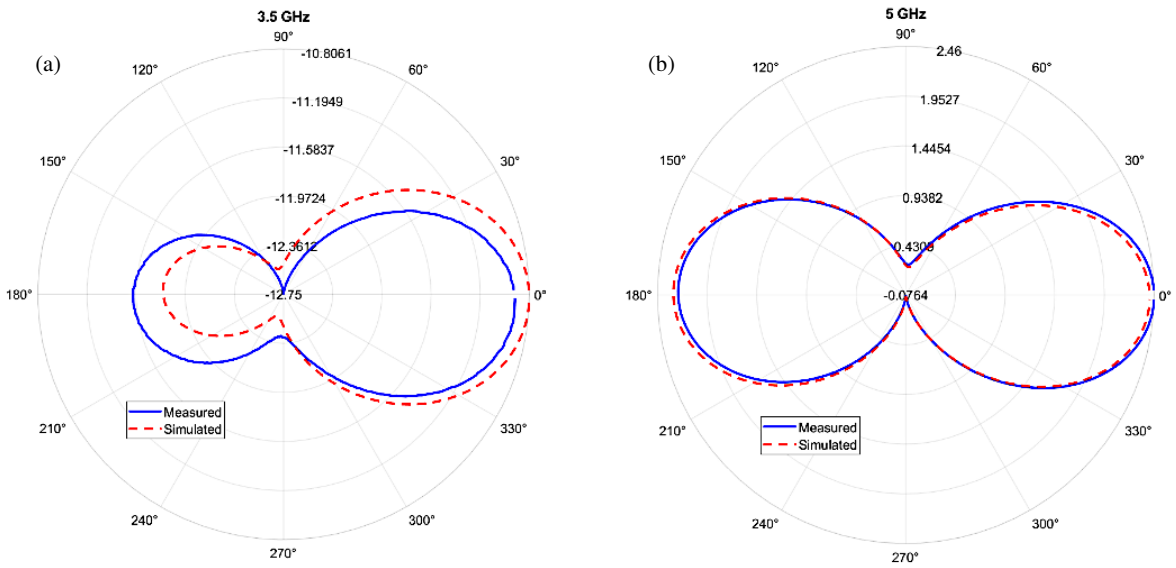

FIGURE 3. Simulated and measured radiation patterns ($\phi = 0°$) at (a) 3.5 and (b) 5 GHz.

TABLE 1. Design parameters for the single antenna element.

Parameter	Value (mm)
w	13
l	7
ws	11
ls	3.3
t	0.7
c	1
le	4.5
re	5.5
we	3
$w2$	26
$l2$	26
$ws2$	20
$ls2$	10
ms	13

rejection around these points. The 5.5 GHz-specific notch confirms that WLAN band suppression is successfully obtained by employing the inverted C-slot design. Overall, the S_{11} response confirms that the antenna is a promising candidate for UWB applications with band-notch integration.

2.1.2. Radiation Patterns

Figure 3 shows the simulated and measured radiation patterns of the proposed antenna in the H-plane ($\phi = 0°$) at 3.5 GHz and 5 GHz, both within the desired passbands of the UWB range. The antenna exhibits quasi-omnidirectional characteristics in this plane, which is desirable for typical UWB communication scenarios. The good agreement between simulation and measurement validates the antenna's performance. These two frequencies were deliberately selected to illustrate the radiation behavior below and above the notched bands (WiMAX and WLAN). The frequency of 5.5 GHz lies within the designed notched band (WLAN), where the antenna is intended to suppress radiation to mitigate interference. At this frequency, the antenna's gain and efficiency are greatly reduced due to the band-rejection mechanism. Therefore, radiation patterns at 5.5 GHz are not plotted, as the antenna is effectively "off" at that frequency. The slight deviations between measured and simulated results may be attributed to fabrication tolerances, cable effects, and measurement environment.

2.1.3. Radiation Efficiency

As shown in Fig. 4(a), very good agreement between simulated and measured radiation efficiency is observed throughout the entire UWB for the designed antenna. The radiation efficiency is more than 90% over most of the band, indicating very low loss of input power and very efficient radiation. Sharp efficiency notches are observed around 3.5 GHz and 5.5 GHz, where the measured efficiency is reduced to around 10–30%. These deep notches actually occur at intended notch bands, thus establishing that the unwanted radiation rejection at selected bands (such as WiMAX and WLAN bands) is possible with the design. Good agreement between measured and simulated curves throughout the rest of band is a sign of good design performance and a good prospective candidate for UWB applications with intended interference rejection.

2.1.4. Realized Gain

Experimental and simulated curves of realized gain in Fig. 4(b) have a close resemblance throughout the UWB. The antenna realizes a peak gain of 4 to 5 dBi over a vast range of intended working frequencies, signifying robust directional performance and gain stability. Similar to that in the plot of efficiency, a gain decline is noted at approximately 3.5 GHz and 5.5 GHz showing two identifiable dips in gain, with a measured decline approximately -10 dBi and -4 dBi, respectively. These reductions fall spot-on over unwanted notch bands, affirming the se-

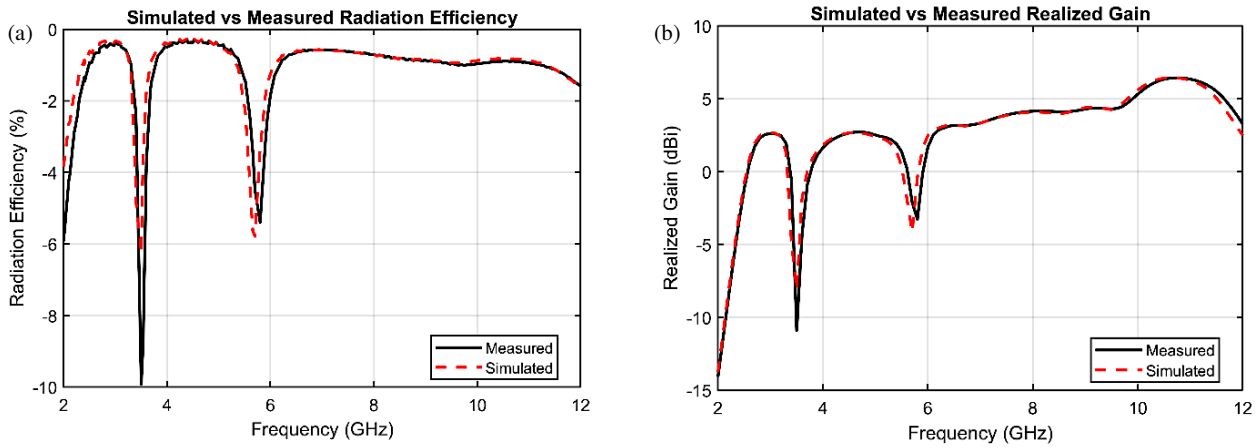

FIGURE 4. Radiation characteristics of the single UWB antenna: (a) Radiation efficiency across frequency. (b) Peak gain across frequency.

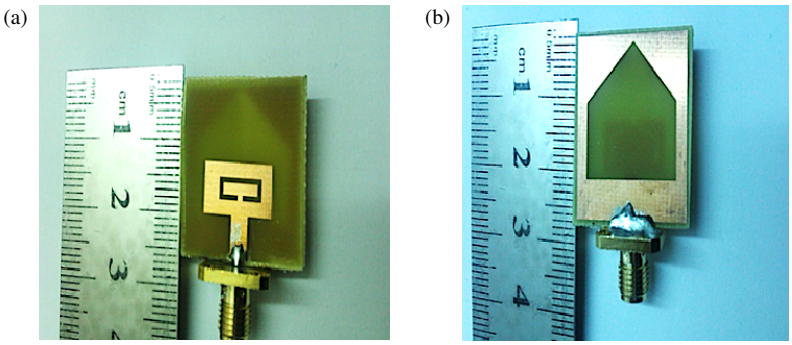

FIGURE 5. Photographs of the fabricated modified UWB antenna with WLAN notch. (a) Top view. (b) Bottom view.

lective attenuation ability of the antenna. This gain suppression around notch frequencies points to the expertise of the antenna in seriously plummeting reception and radiation of signals over undesired bands. The overall behavior resemblance of gain throughout the rest of the band ensures that the antenna is a suitable candidate for wideband communication systems that require uninterrupted gain and band-specific rejection.

2.2. Fabricated Prototype

For confirmation of simulation results, a single UWB antenna is developed over a 1.5 mm thickness FR4 substrate with a loss tangent of 0.025 and a relative permittivity $\varepsilon_r = 4.5$. Excitation is through a standard 50 Ω microstrip line. The developed prototype is illustrated in Fig. 5. Vector network analyzer is used to test the antenna, and corresponding measured results are noted to have good agreement with expected performance according to simulations. In particular, both dual notches around 3.5 GHz and 5.5 GHz are clearly seen to confirm that good rejection of interference arising from the WLAN and WiMAX bands is indeed achieved by the antenna while still providing wideband operation over much of the remainder of the band.

3. THE PROPOSED 4-PORT MIMO ANTENNA

The MIMO antenna design is shown in Fig. 6. An electromagnetic bandgap (EBG) structure is utilized between the antenna elements, and a vertical via (0.5 mm diameter) is utilized to connect the top EBG patch to the ground plane. The EBG is utilized twice in this design, and it minimizes mutual coupling between contiguous elements by restricting surface current propagation and produces a notch function at 5.5 GHz, equivalent to the WLAN band. As a result, a level of isolation approximately 18 dB is attained without utilizing external filters or decoupling components. The 3.5 GHz WiMAX band is targeted through a notch function provided by the inverted C-slot used in every radiating element. The EBG and slot-based schemes are utilized together to provide good dual-band interference rejection, good isolation, and compact MIMO operation.

3.1. Effect of EBG on Isolation

To evaluate EBG structure's influences over MIMO antenna performance, a comparison has been conducted between designs featuring and not featuring EBG. As suggested in Fig. 7(a) for S_{12}, Fig. 7(b) for S_{13}, and Fig 7(c) for S_{14}, sequentially incorporating EBG significantly enhances isolation between antenna elements with apparent mutual coupling suppression throughout the UWB. As a matter of fact, the isolation in S_{12} is significantly improved from approximately -20 dB to below -30 dB at certain frequencies when an EBG is introduced. Similar trends are observed in S_{13} and S_{14}, and therefore are confirmed to test that EBG is indeed capable of surface currents suppression between ports. Interestingly, reflection coefficient

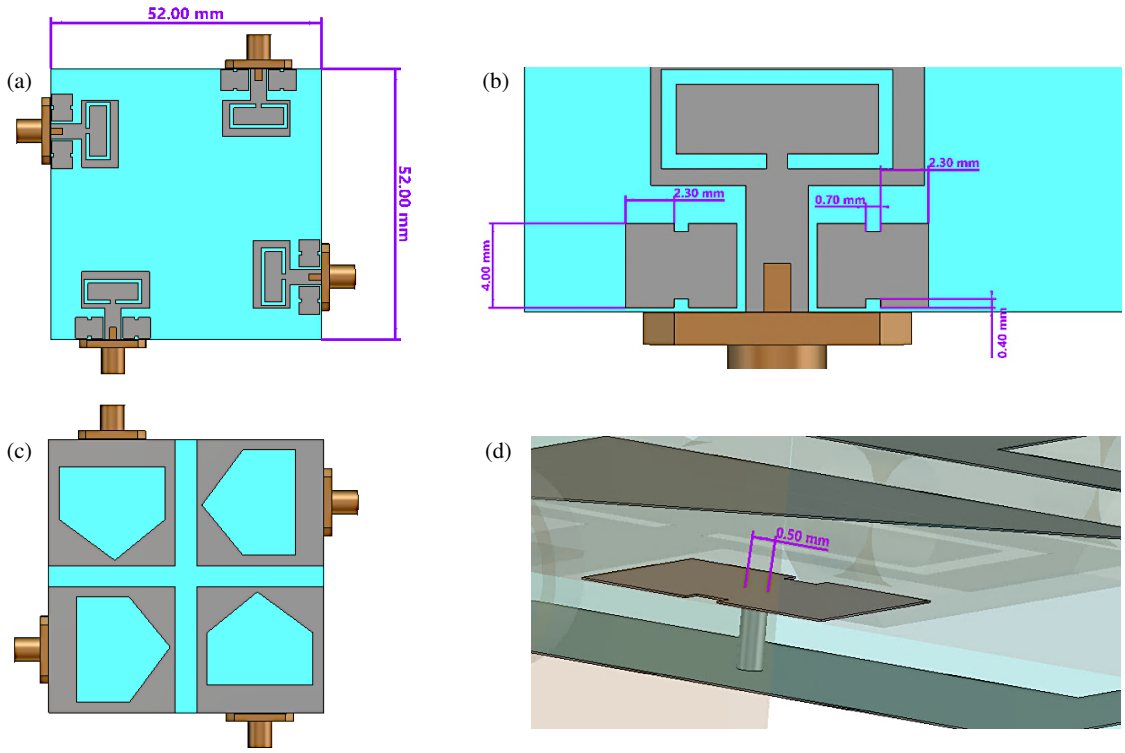

FIGURE 6. 4-port MIMO. (a) Top view. (b) Back view. (c) EBG dimensions. (d) EBG wire diameter.

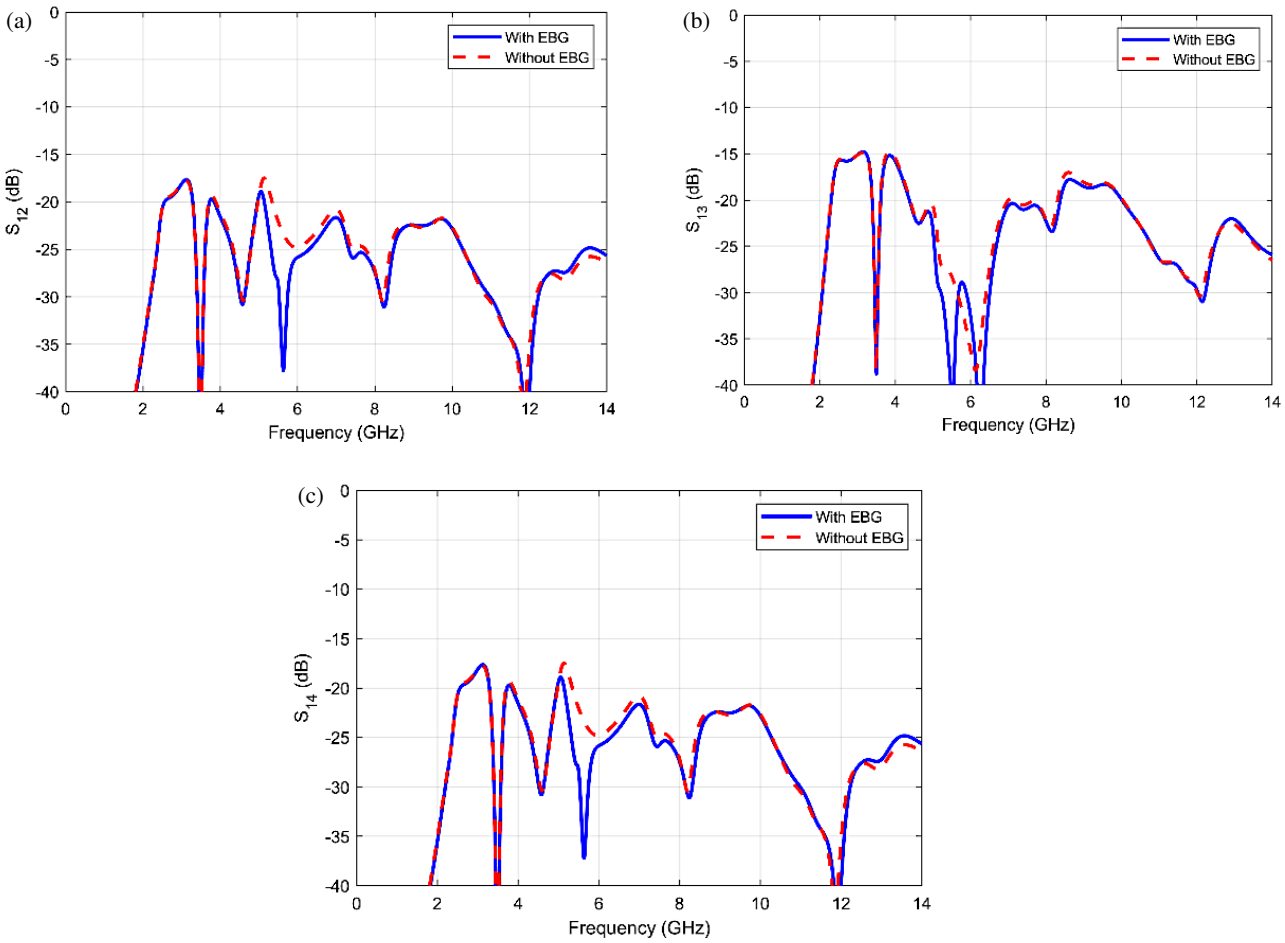

FIGURE 7. Isolation comparison between MIMO antennas with and without EBG: (a) S_{12}, (b) S_{13}, (c) S_{14}.

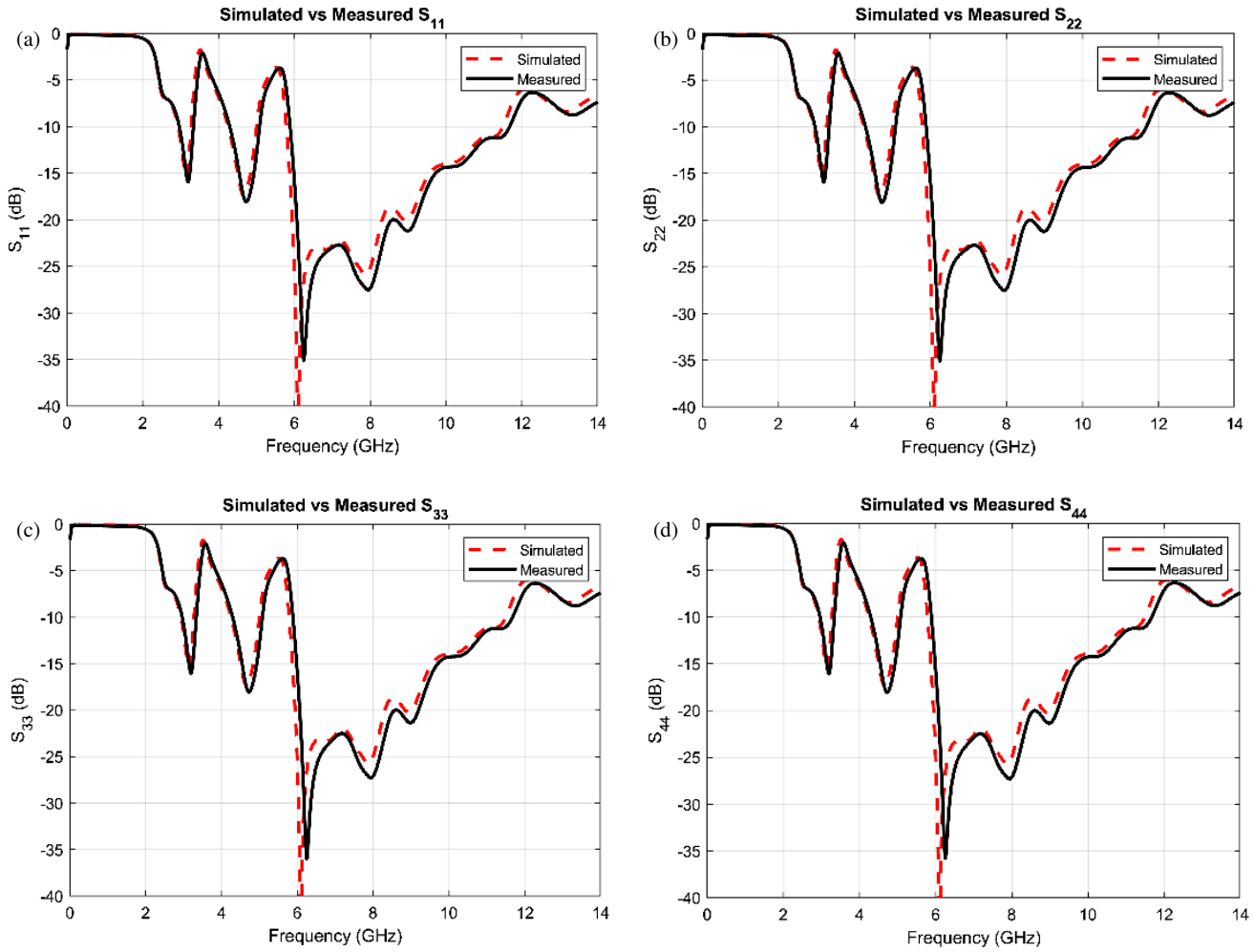

FIGURE 8. Simulated vs. measured reflection coefficients (a) S_{11}, (b) S_{22}, (c) S_{33}, (d) S_{44}.

(S_{11}) is maintained approximately unchanged between the two designs and therefore demonstrates that EBG enhances isolation without compromising impedance matching. These results are a good sign that EBG structure is indeed capable of simultaneously supporting isolation enhancement and notch-band operation, and consequently contributing towards overall UWB MIMO antenna performance.

3.2. Performance Evaluation: Simulated vs. Measured

3.2.1. Reflection Coefficients

The reflection responses of 4-port MIMO antennas were characterized both by full-wave simulation and measurement, as shown in Figs. 8(a)–(d) for S_{11}, S_{22}, S_{33}, and S_{44}, respectively. For every port, good correspondence between simulated (dashed red) and measured (solid black) data is noted. The antenna covers a -10 dB impedance bandwidth over approximately 2.6 GHz to 12.6 GHz, excluding both notched bands, indicating wideband operation over most of the UWB. Both clearly differentiated notches are at 3.5 GHz and 5.5 GHz, corresponding to the WiMAX and WLAN bands, respectively. More specifically, the rejection band of WiMAX spans 3.3 GHz to 3.7 GHz, whereas WLAN notch band spans 5.1 GHz to 5.9 GHz, clearly showing high-Q band rejection behavior. These stopbands are observable in all four of the reflection curves and confirm the filtering feature incorporated in the antenna. Small discrepancy between simulated and measured responses above 11 GHz is likely due to connector loss or fabrication tolerance, but overall reflection response shows suitability of the antenna to UWB applications.

3.2.2. Isolation

The isolation characteristics between port 1 and others are depicted in Figs. 9(a)–(c) for S_{12}, S_{13}, and S_{14}, respectively. For all cases, the isolation is found to be below -20 dB throughout most of the UWB, verifying good decoupling between elements. Significant isolation enhancement is observed around notch bands, where isolation is equal to or greater than -30 dB, namely around 3.5 GHz and 5.5 GHz rejection bands. This finding serves as a verification of a fact that not only does the geometry of the antenna, through use of a part of electromagnetic bandgap (EBG) component, create a dual-band notch characteristic but also enhance port-to-port isolation. The good correlation between theoretical and experimental isolation curves serves as a verification of design validity and real-world operation of a MIMO-UWB system.

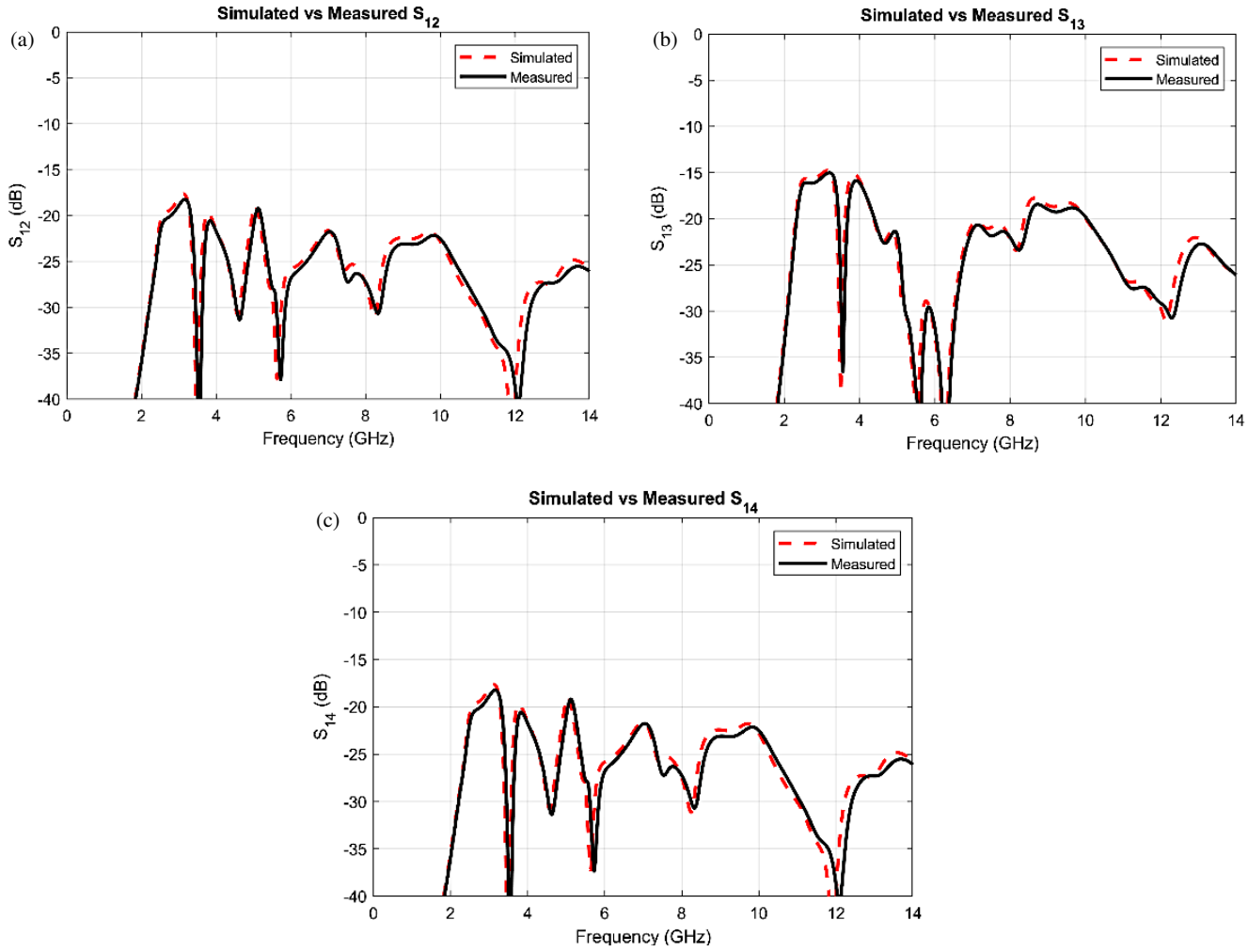

FIGURE 9. Simulated vs. measured transmission coefficients (a) S_{12}, (b) S_{13}, (c) S_{14}.

3.2.3. Total Active Reflection Coefficient (TARC)

Figure 10(a) shows the simulated total active reflection coefficient (TARC) of the UWB-MIMO antenna under various excitation phase angles (0°–180°). The total active reflection coefficient (TARC) maintains values below −10 dB throughout the 3.1–10.6 GHz range, except for the notched bands at approximately 3.5 GHz and 5.5 GHz. This performance indicates effective multi-port impedance matching and high radiation efficiency. Pronounced peaks in the TARC response at these frequencies validate the dual-band rejection targeting the WiMAX and WLAN bands, respectively. Such low TARC values outside the notches are comparable to those reported in recent compact MIMO designs [7], indicating that the antenna maintains good matching under active excitation. Additionally, Fig. 10(b) compares the simulated and measured average TARCs. The measured curve closely follows the simulated one, including the locations and depths of the dual notches. Crucially, both simulation and measurement show TARC below −10 dB over nearly the entire UWB range, except at the notch bands. This strong simulation-measurement agreement confirms the validity of the design and fabrication. The agreement of TARC profiles further demonstrates that the modeled multi-port behavior accurately predicts the real antenna performance.

3.2.4. Envelope Correlation Coefficient & Diversity Gain

The envelope correlation coefficient (ECC) values plotted in Fig. 11(a) confirm very low mutual correlation between antenna elements. Across the operational band (excluding notched regions), the ECC remains well below 0.05, satisfying the requirement for effective MIMO operation (ECC < 0.5). The average ECC is < 0.005, and the EBG structure significantly contributes to minimizing surface current coupling, thereby enhancing isolation and lowering ECC. Furthermore, Fig. 11(b) shows the diversity gain (DG) for port pairs 1–2, 1–3, and 2–3. All three DG curves lie around 9.9–10.0 dB across the UWB, essentially reaching the theoretical maximum of 10 dB for two uncorrelated antennas. Only at the notch frequencies (where the ECC briefly rises) does DG dip slightly below 9.9 dB. The overall DG $\approx$ 10 dB directly follows from the negligible ECC and confirms that the antenna provides near-ideal spatial diversity. This high DG is in line with the low ECC observed above and matches reported results for high-performance UWB-MIMO antennas [8].

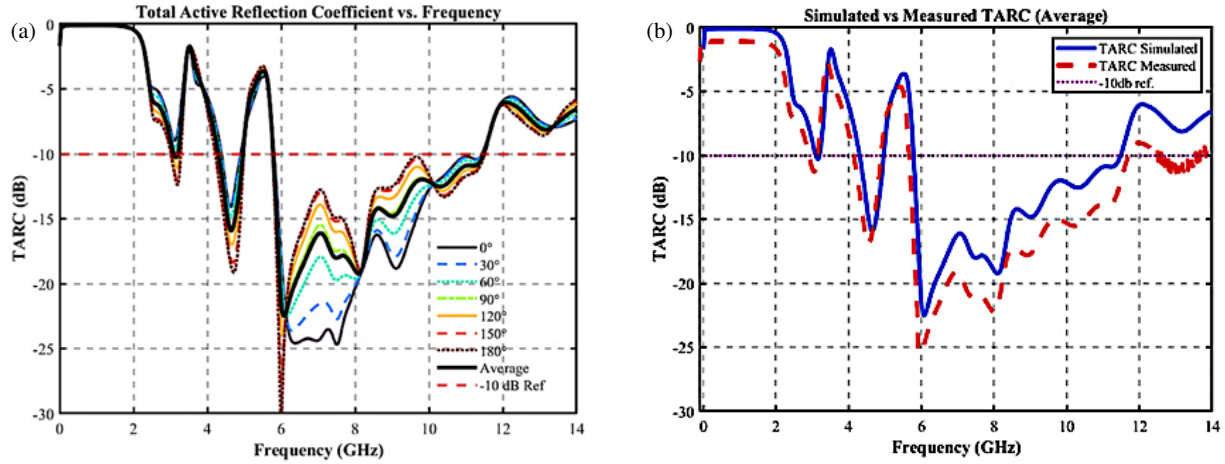

FIGURE 10. TARC performance of the MIMO antenna. (a) Simulated TARC under various excitation phases (0°–180°). (b) Simulated and measured average TARC.

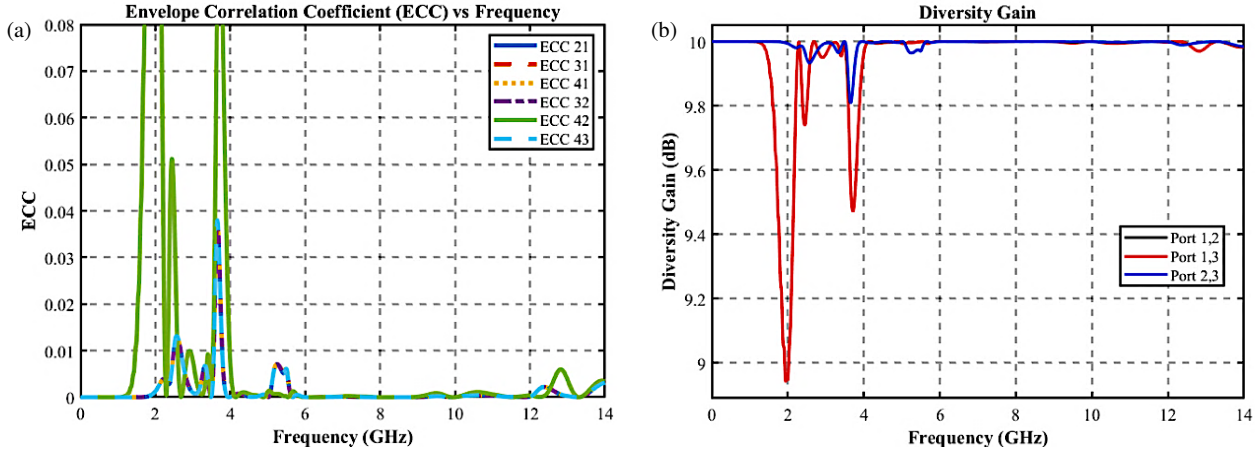

FIGURE 11. MIMO performance metrics of the proposed antenna. (a) Envelope correlation coefficient (ECC) for all port combinations. (b) Diversity gain.

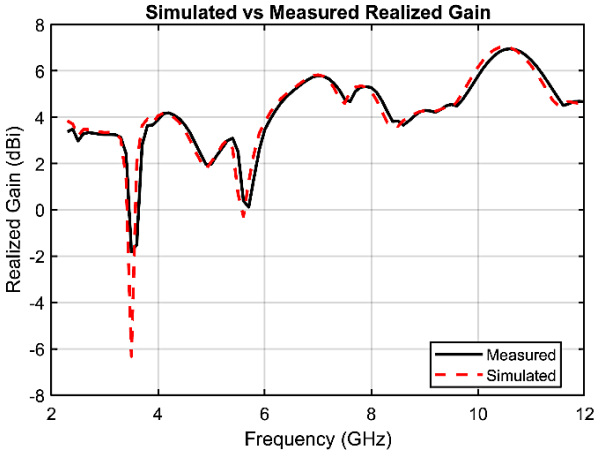

FIGURE 12. Simulated vs. measured realized gain.

3.2.5. Realized Gain

Figure 12 shows both the measured and simulated realized gains of the desired UWB MIMO antenna over 2–12 GHz. The plots show good correspondence between the two data sets, justifying both design accuracy and prototype consistency. The realized gain is somewhat steady between 3 and 7 dBi throughout most of bands, with two deep nulls seen prominently. The first deep drop is at around 3.5 GHz, whereupon the gain achieves a level around -6.5 dBi, and the second is seen at around 5.5 GHz, corresponding to intended notched bands to suppress WiMAX and WLAN interference. Beyond these notches, a smooth gain characteristic is seen with a steady performance, reaching a peak gain level around 7 dBi, which is well within that anticipated for a compact monopole UWB antenna. The good correspondence between the two gain curves further proves both design effectiveness and robustness.

3.2.6. Radiation Pattern

The directionality characteristic of 4-port UWB MIMO antenna is determined through simulated and measured far-fields of Antenna 1's radiation patterns at a few major UWB frequencies, e.g., notched bands at 3.5 GHz (WiMAX) and 5.5 GHz (WLAN). The measurement is conducted at 3.5, 5.5, 6, 8, and 10 GHz in E-plane ($\varphi = 0°$) as shown in Fig. 13. The quasi-

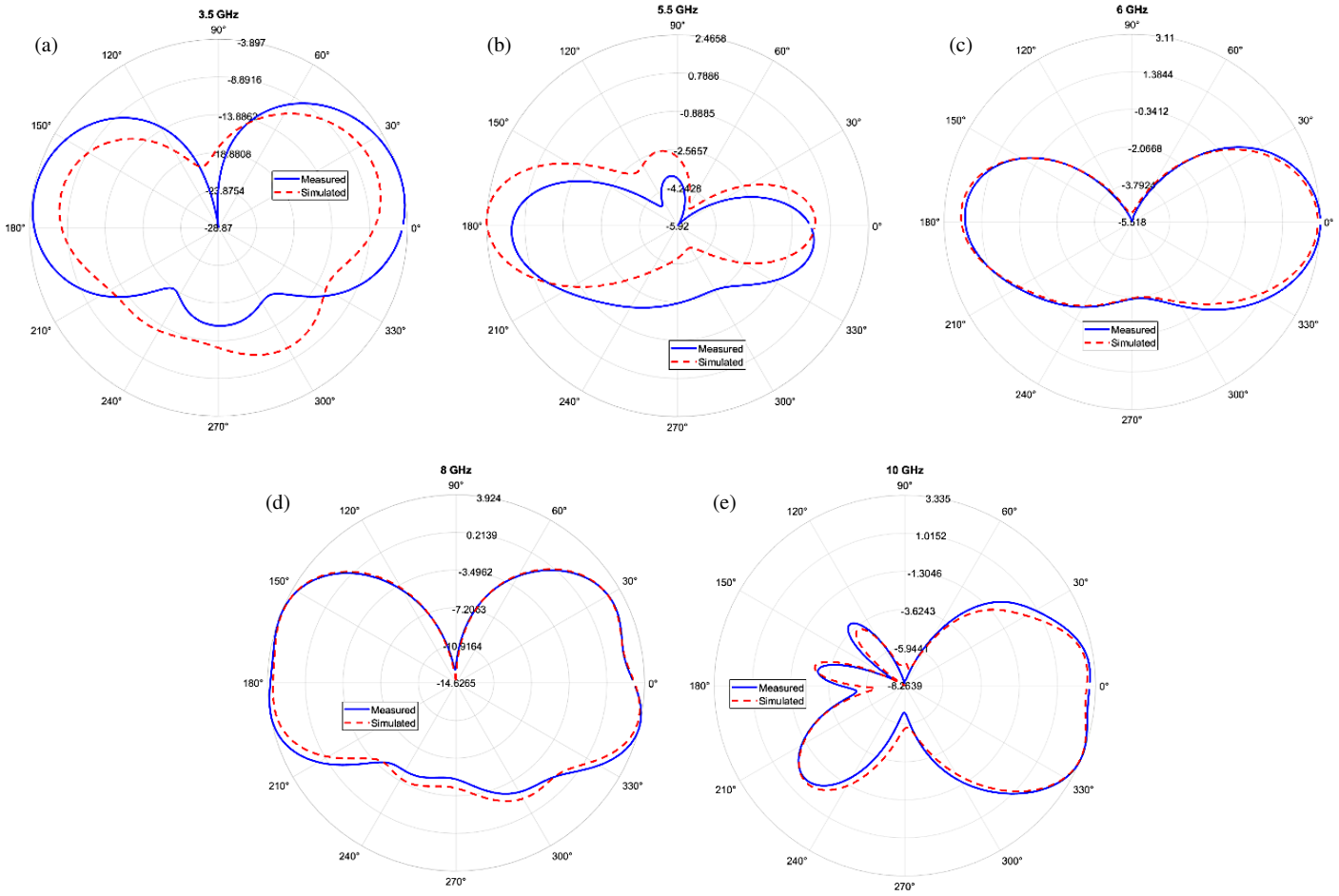

FIGURE 13. Simulated and measured radiation patterns of Antenna 1 at 3.5 GHz, 5.5 GHz, 6 GHz, 8 GHz, and 10 GHz in the E-plane ($\varphi = 0°$).

TABLE 2. Comparison of 4-port UWB-MIMO antennas.

Ref.	Size (mm^3)	ε_r	Frequency Range (GHz)	Notch Bands (GHz)	Isolation (dB)	Peak Gain (dBi)	Efficiency (%)	ECC
[1]	$47 \times 47 \times 1.6$	4.4	3.0–12.0	3.3–4.3 (WiMAX)	> 22	3.5	85	< 0.005
[3]	$45 \times 40 \times 0.97$	4.4	3.1–10.6	4.6–5.9 (WLAN), 6.8–8.8 (X-band)	> 22	6.1	88	< 0.01
[9]	$66.2 \times 66.2 \times 1.44$	4.4	2.08–10.4	2.27–3.62 (Bluetooth/LTE/WiMAX)	> 20	9.6	90	< 0.05
[10]	$32.3 \times 32.3 \times 0.8$	4.4	3.1–12.0	4.5–5.5 (WLAN)	> 15	5.0	80	< 0.02
This work	$52 \times 52 \times 1.5$	4.5	3.1–10.6	3.5 (WiMAX), 5.5 (WLAN)	> 24	7.1	> 90	< 0.005

omnidirectional radiation patterns at lower frequencies like 3.5 GHz and 5.5 GHz are appropriate and applicable in UWB applications, but directive patterns are observed at higher frequencies. Notably, a wide suppression of gain at 3.5 GHz and 5.5 GHz proves successful rejection of WiMAX and WLAN interference through notched band design. The good matching between measured (blue solid line) and simulated (red dashed line) outcomes reveals good agreement and consequently ensures a very good level of design accuracy and very low fabrication and measurement discrepancy. The antenna is very stable with a radiation characteristic over the UWB with distinct nulls at notched bands, thereby supporting not only reliability of design but also performance support.

3.2.7. Current Density

We draw the current density for antenna 1 at different frequencies. Fig. 14(a) shows the current density at 3.5 GHz. We notice that the current is concentrated around the edges of the C-slot, and its resonance at that frequency causes destructive interfer-

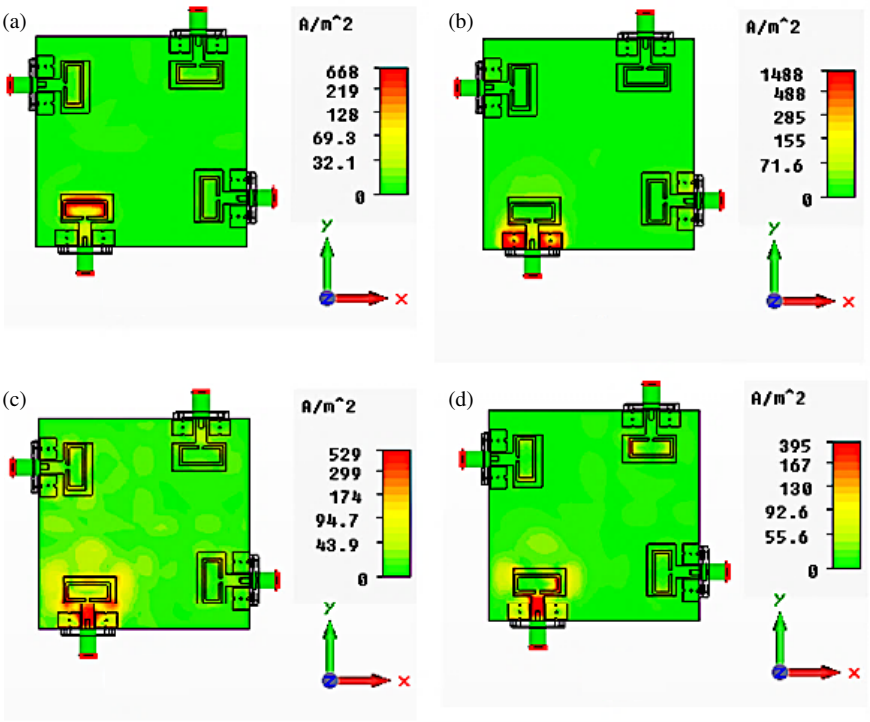

FIGURE 14. Current densities at (a) $f = 3.5$ GHz, (b) $f = 5.5$ GHz, (c) $f = 8$ GHz, (d) $f = 10$ GHz.

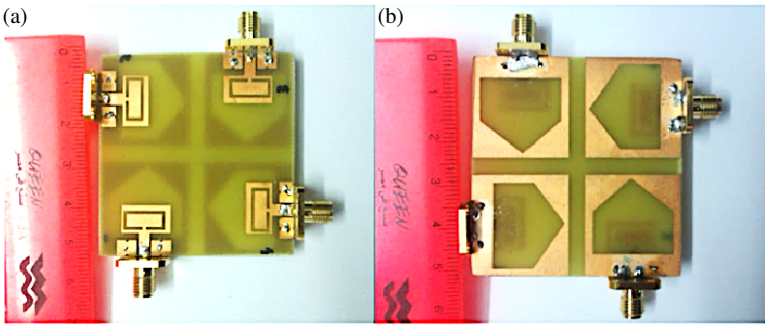

FIGURE 15. Photograph of the fabricated MIMO antenna. (a) Top view. (b) Back view.

ence; hence, a notch is implemented. At frequency 5.5 GHz shown in Fig. 14(b), the current is concentrated around the edges of the EBG, and a notch is constructed. Fig. 14(c) and Fig. 14(d) show the current densities at two different operating frequencies, 8 GHz and 10 GHz, respectively. It is shown that the current in this case is much concentrated on the edges of the radiating patch such that much of the input power is radiated from the antenna.

3.3. Fabricated Version

Figure 15 presents the fabricated prototype of the proposed antenna, which was manufactured using an FR4 substate with a relative permittivity (ε_r) of 4.5 and a thickness of 1.6 mm. The fabricated notched MIMO antenna has a dimension of $52 \times 52 \times 1.6$ mm. Finally, Table 2 shows a comparison of the proposed UWB-MIMO antenna with other UWB-MIMO antennas.

4. CONCLUSION

This work successfully demonstrates a miniaturized 4-port UWB-MIMO antenna with dual band-notched features for the suppression of WiMAX (3.5 GHz) and WLAN (5.5 GHz) interference. The suggested design produces a compact four-port UWB-MIMO antenna size of $52 \times 52 \times 1.5$ mm^3 with an FR4 substrate, making it a low-cost solution for feasible applicability. Employing EBG structures and an inverted C-slot, the antenna realizes excellent inter-port isolation (> 24 dB) and steep dual-frequency rejections without adding additional filters or complicated decoupling techniques. Highlighted performance metrics have a wide UWB operational band (3.1–10.6 GHz), a stable radiating gain (3.5–7.2 dBi), and radiation efficiency suppression ($< 20\%$) at a notched band, which confirms effective interference suppression. Simulations are strongly supported by measurement, with expected impedance matching (VSWR < 2), maintaining ECC values well below 0.005 for optimal isolation and nearly ideal diversity gain (10 dB). Radi-

ation patterns verify quasi-omnidirectional patterns, making it an excellent choice for various UWB applications.

ACKNOWLEDGEMENT

The authors would like to thank Universiti Teknikal Malaysia Melaka (UTeM) and the Ministry of Higher Education (MOHE) of Malaysia for supporting this project.

REFERENCES

[1] Ibrahim, A. A. and M. F. A. Sree, "UWB MIMO antenna with 4-element, compact size, high isolation and single band rejection for high-speed wireless networks," *Wireless Networks*, Vol. 28, No. 7, 3143–3155, 2022.

[2] Al-Gburi, A., Z. Zakaria, M. Palandoken, I. M. Ibrahim, A. Althuwayb, S. Ahmad, and S. S. Al-Bawri, "Super compact UWB monopole antenna for small IoT devices," *Comput. Mater. Contin.*, Vol. 73, No. 3, 2785–2799, 2022.

[3] Kumar, P., T. Ali, S. Pathan, K. Nayak, T. Khan, A. A. Kishk, *et al.*, "A quad port dual band notch UWB MIMO antenna using hybrid decoupling structure," *Results in Engineering*, Vol. 23, 102551, 2024.

[4] Saritha, V., V. N. K. R. Devana, M. B. Lakshmi, M. A. Halimi, G. Devi, N. R. Lavuri, and A. J. A. Al-Gburi, "Low-profile four-port MIMO antenna realizing penta-band notches for UWB systems," *Optik*, Vol. 336, 172454, 2025.

[5] Kumar, A., G. Singh, M. K. Abdulhameed, S. R. Hashim, and A. J. A. Al-Gburi, "Development of fractal 5G MIMO antenna for sub 6 GHz wireless automotive applications," *Progress In Electromagnetics Research M*, Vol. 130, 121–128, 2024.

[6] Thakur, E., N. Jaglan, A. Gupta, and A. J. A. Al-Gburi, "Multi-band notched circular polarized MIMO antenna for ultra-wideband applications," *Progress In Electromagnetics Research M*, Vol. 125, 87–95, 2024.

[7] Kumar, P., A. K. Singh, R. Kumar, R. Sinha, S. K. Mahto, A. Choubey, and A. J. A. Al-Gburi, "High isolated defected ground structure based elliptical shape dual element MIMO antenna for S-band applications," *Progress In Electromagnetics Research C*, Vol. 143, 67–74, 2024.

[8] Sharma, M., V. Dhasarathan, S. K. Patel, and T. K. Nguyen, "An ultra-compact four-port 4×4 superwideband MIMO antenna including mitigation of dual notched bands characteristics designed for wireless network applications," *AEU — International Journal of Electronics and Communications*, Vol. 123, 153332, 2020.

[9] Mohanty, A. K., S. Mishra, and M. Panigrahi, "Four-port triple band notched UWB-MIMO antenna for 5G and IoT applications," *Wireless Personal Communications*, Vol. 123, No. 1, 107–122, 2022.

[10] Kareem, Q. H. and M. J. Farhan, "Compact quad-port UWB-MIMO antenna with single band-notch using octagonal design," *Wireless Personal Communications*, Vol. 123, No. 2, 1419–1436, 2022.

[11] Jhunjhunwala, V. K., P. Kumar, A. P. Parameswaran, P. R. Mane, O. P. Kumar, T. Ali, S. Pathan, S. Vincent, and P. Kumar, "A four port flexible UWB MIMO antenna with enhanced isolation for wearable applications," *Results in Engineering*, Vol. 24, 103147, 2024.

[12] Mohamed, H. A. and M. Aboualalaa, "A low profile super UWB-MIMO antenna with D-shaped for satellite communications, 5G and beyond applications," *Scientific Reports*, Vol. 15, No. 1, 15660, 2025.

[13] Irshad Khan, M., M. I. Khattak, S. Ur Rahman, A. B. Qazi, A. A. Telba, and A. Sebak, "Design and investigation of modern UWB-MIMO antenna with optimized isolation," *Micromachines*, Vol. 11, No. 4, 432, 2020.

[14] Dkiouak, A., M. E. Ouahabi, S. Chakkor, M. Baghouri, A. Zakriti, and Y. Lagmich, "High performance UWB MIMO antenna by using neutralization line technique," *Progress In Electromagnetics Research C*, Vol. 131, 185–195, 2023.

[15] Govindan, T., S. K. Palaniswamy, M. Kanagasabai, S. Kumar, T. R. Rao, and M. G. N. Alsath, "Conformal quad-port UWB MIMO antenna for body-worn applications," *International Journal of Antennas and Propagation*, Vol. 2021, No. 1, 9409785, 2021.

[16] Rahim, S., A. A. Elobied, W. Huang, and X.-X. Yang, "Super-UWB MIMO antenna with dual band-notched and high gain," *Radio Science*, Vol. 57, No. 11, 1–9, 2022.

[17] Abbas, A., N. Hussain, M. A. Sufian, W. A. Awan, J. Jung, S. M. Lee, and N. Kim, "Highly selective multiple-notched UWB-MIMO antenna with low correlation using an innovative parasitic decoupling structure," *Engineering Science and Technology, An International Journal*, Vol. 43, 101440, 2023.

[18] Tighilt, Y., C. Bensid, D. Sayad, S. Mekki, R. Zegadi, M. L. Bouknia, I. Elfergani, P. Singh, J. Rodriguez, and C. Zebiri, "Low-profile UWB-MIMO antenna system with enhanced isolation using parasitic elements and metamaterial integration," *Electronics*, Vol. 12, No. 23, 4852, 2023.

[19] Al Gburi, A. J. A., "5G MIMO antenna: Compact design at 28/38 GHz with metamaterial and SAR analysis for mobile phones," *Przegląd Elektrotechniczny*, Vol. 100, No. 4, 171–174, 2024.

[20] Wang, M., J. Nan, and J. Liu, "High-isolation UWB MIMO antenna with multiple X-shaped stubs loaded between ground planes," *International Journal of Antennas and Propagation*, Vol. 2021, No. 1, 1155471, 2021.

[21] Ibrahim, A. A., M. I. Ahmed, and M. F. Ahmed, "A systematic investigation of four ports MIMO antenna depending on flexible material for UWB networks," *Scientific Reports*, Vol. 12, No. 1, 14351, 2022.

[22] Khan, M. S., S. A. Naqvi, A. Iftikhar, S. M. Asif, A. Fida, and R. M. Shubair, "A WLAN band-notched compact four element UWB MIMO antenna," *International Journal of RF and Microwave Computer-Aided Engineering*, Vol. 30, No. 9, e22282, 2020.

[23] Pannu, P. and D. K. Sharma, "A low-profile quad-port UWB MIMO antenna using defected ground structure with dual notch-band behavior," *International Journal of RF and Microwave Computer-Aided Engineering*, Vol. 30, No. 9, e22288, 2020.

[24] Wu, A., M. Zhao, P. Zhang, and Z. Zhang, "A compact four-port MIMO antenna for UWB applications," *Sensors*, Vol. 22, No. 15, 5788, 2022.

[25] Salehi, M. and H. Oraizi, "Wideband high gain metasurface-based 4T4R MIMO antenna with highly isolated ports for sub-6 GHz 5G applications," *Scientific Reports*, Vol. 14, No. 1, 14448, 2024.

[26] Kumari, T., A. Senapati, and A. N. Ghazali, "A UWB-specific metasurface-inspired MIMO antenna with enhanced isolation and gain," in *Proceedings of the 1st International Conference on Cognitive & Cloud Computing (IC3Com 2024)*, 30–36, Jaipur, India, 2024.

[27] Sharma, A., S. Sharma, V. Sharma, G. Wadhwa, and R. Kumar, "A compact ultra-wideband millimeter-wave four-port multiple-input multiple-output antenna for 5G internet of things applications," *Sensors*, Vol. 24, No. 22, 7153, 2024.